RESEARCH ARTICLE

NMR IN BIOMEDICINE WILEY

Docetaxel chemotherapy response in PC3 prostate cancer mouse model detected by rotating frame relaxations and water diffusion

Hanne Laakso[1] | Elias Ylä-Herttuala[1] | Alejandra Sierra[1] | Ivan Jambor[2,3] | Matti Poutanen[4] | Heidi Liljenbäck[4,5] | Helena Virtanen[5] | Harri Merisaari[2,6] | Hannu Aronen[2,7] | Heikki Minn[5,8] | Anne Roivainen[4] | Timo Liimatainen[1,9,10]

[1]A.I. Virtanen Institute for Molecular Sciences, University of Eastern Finland, Kuopio, Finland

[2]Department of Radiology, University of Turku, Turku, Finland

[3]Department of Radiology, Icahn School of Medicine at Mount Sinai, New York, NY, USA

[4]Turku Center for Disease Modeling, University of Turku, Turku, Finland

[5]Turku PET Centre, University of Turku and Turku University Hospital, Turku, Finland

[6]Department of Future Technologies, University of Turku, Turku, Finland

[7]Medical Imaging Centre of Southwest Finland, Turku University Hospital, Turku, Finland

[8]Department of Oncology and Radiotherapy, Turku University Hospital, Turku, Finland

[9]Research Unit of Medical Imaging, Physics and Technology, University of Oulu, Oulu, Finland

[10]Department of Clinical Radiology, Oulu University Hospital, Oulu, Finland

Correspondence
Timo Liimatainen, Research Unit for Medical Imaging, Physics and Technology, University of Oulu/Oulu University Hospital, PO Box 50, FI-70029 Oulu, Finland.
Email: timo.liimatainen@oulu.fi

MRI is a common method of prostate cancer diagnosis. Several MRI-derived markers, including the apparent diffusion coefficient (ADC) based on diffusion-weighted imaging, have been shown to provide values for prostate cancer detection and characterization. The hypothesis of the study was that docetaxel chemotherapy response could be picked up earlier with rotating frame relaxation times T_{RAFF2} and T_{RAFF4} than with the continuous wave $T_{1\rho}$, adiabatic $T_{1\rho}$, adiabatic $T_{2\rho}$, T_1, T_2 or water ADC. Human PC3 prostate cancer cells expressing a red fluorescent protein were implanted in 21 male mice. Docetaxel chemotherapy was given once a week starting 1 week after cell implantation for 10 randomly selected mice, while the rest served as a control group (n = 11). The MRI consisted of relaxation along a fictitious field (RAFF) in the second (RAFF2) and fourth (RAFF4) rotating frames, T_1 and T_2, continuous wave $T_{1\rho}$, adiabatic $T_{1\rho}$ and adiabatic $T_{2\rho}$ relaxation time measurements and water ADC. MRI was conducted at 7 T, once a week up to 4 weeks from cell implantation. The tumor volume was monitored using T_2-weighted MRI and optical imaging. The histology was evaluated after the last imaging time point. Significantly reduced RAFFn, $T_{1\rho}$, $T_{2\rho}$ and conventional relaxation times 4 weeks after tumor implantation were observed in the treated tumors compared with the controls. The clearest short- and long-term responses were obtained with T_1, while no clear improvement in response to treatment was detected with novel methods compared with conventional methods or with RAFFn compared with all others. The tumor volume decreased after a two-week time point for the treated group and increased significantly in the control group, which was supported by increasing red fluorescent light emission in the control tumors. Decreased relaxation times were associated with

successful chemotherapy outcomes. The results indicate altered relaxation mechanisms compared with higher dose chemotherapies previously published.

KEYWORDS

cancer, follow-up, prostate, relaxation, rotating frame, therapy, water diffusion

1 | BACKGROUND

According to the Finnish cancer registry, the number of new prostate cancers diagnosed per year is the largest among all cancer incidences. New cases of prostate cancers amount in Finland to 4925 cases per year and in Nordic countries to 24 842 cases per year (statistics from 2012 to 2016) with the number of deaths amounting to 875 and 5490 patients, respectively.[1] Prostate cancer makes up 30% of all cancers in Finland, impacts numerous individuals and causes a noticeable economic burden. The variety of therapy options for prostate cancer includes prostatectomy, radiation-, cryo- and hormone-chemotherapies, and vaccine treatment.

Prostate cancer has traditionally been diagnosed based on a prostate specific antigen and digital rectal examination.[2] Ultrasound (US) is used for biopsy guidance after positive digital rectal examination results or elevated prostate specific antigen.[3] Typically, prostate cancer is hypoechoic with increased vascularity from a Doppler US. However, neither of these markers is highly sensitive or specific to prostate cancer. US-based elastography, especially quantitative shear-wave elastography, increases the sensitivity and negative predictive value remarkably.[3] Additionally, the sensitivity may be improved by measuring the microvasculature using contrast-enhanced US.[3] Over the last 10 years, prostate multiparametric MRI has been increasingly used for the detection and characterization of prostate cancer. Prostate multiparametric MRI usually consists of T_2-weighted imaging and one or more of the following methods: diffusion-weighted imaging, dynamic contrast-enhanced MRI, and optional proton (^{1}H) MRS. Multislice T_2-weighted imaging provides a good anatomical overview, while specificity and sensitivity to detect aggressive cancer are enhanced by quantitative water diffusion measurement provided by diffusion-weighted imaging, dynamic contrast-enhanced MRI to assess tissue perfusion and ^{1}H MRS to obtain citrate and choline fractions of the total spectroscopy signal.[4–6]

Rotating frame relaxations are specifically sensitive to changes in slow molecular motions that are in the range of low field T_1, providing an opportunity to assess molecular motions that are hindered in T_1, T_2 and water diffusion. As T_1 is sensitive to the motional regime close to the Larmor frequency, high field strengths of several tesla mean that T_1 is sensitive to free water tumbling frequencies in the megahertz range. The longitudinal relaxation time in the rotating frame ($T_{1\rho}$) can be used to measure slow molecular motions in the range from 100 Hz to a few kilohertz at high field strengths. It is sensitive to processes in the intermediate and slow molecular motion regime, for instance ^{1}H chemical exchange between water and hydroxyl, amine or amide groups. $T_{1\rho}$ has been demonstrated to be an early marker of cell death in a rat glioma model.[7,8] The sensitive regime depends on the applied B_1 (kHz range) field, thus enabling more specific probing of slow motion than for example using T_2, which contains contributions from all slow molecular motions non-specifically. To measure rotating frame relaxations more robustly, a method based on relaxation during adiabatic pulses was introduced for $T_{1\rho}$ and transversal relaxation time $T_{2\rho}$.[9,10] With the adiabatic methods, the effective field varies during the pulses, which broadens the range of frequencies that are covered in comparison with continuous wave $T_{1\rho}$, where a single value of effective field is utilized.

Both adiabatic $T_{1\rho}$ and $T_{2\rho}$ were applied to measure a herpes simplex virus thymidine kinase gene transfected BT4C rat glioma undergoing gene therapy induced by ganciclovir.[11] Later, the specific absorption rate of rotating frame relaxation was reduced by the introduction of methodology involving relaxation along a fictitious field (RAFF).[12] The reduction of specific absorption rate is important to maintain the feasibility of rotating frame relaxation measurement especially in humans at 3 T and above. The RAFF relaxation time (T_{RAFF}) was found to correlate well with the cell density in rat gliomas during ganciclovir gene therapy.[13]

In a study that included 50 prostate cancer patients who underwent 3 T MRI before prostatectomy, RAFF was found to outperform various diffusion-weighted imaging acquisitions and T_2 in detecting prostate tumor aggressiveness when compared with the Gleason score from prostatectomy specimens.[14] Gleason score/Gleason grade group is a commonly used histopathological grading system of prostate cancer aggressiveness.[15] T_{RAFF} and $T_{1\rho}$ were shown to be repeatable in patients with prostate cancer at 3 T.[16] A further decrease of the specific absorption rate was achieved with RAFF in the nth rotating frame (RAFFn), which takes further advantage of the RF sweep generated by the fictitious magnetic field.[17] However, this methodology has not been applied either to prostate cancer diagnostic imaging or to treatment response studies. RAFFn holds the potential to assess treatment responses via changes in low molecular motions, for example arising from proton exchange, with smaller specific absorption rate than in RAFF or $T_{1\rho}$.

Docetaxel is a commonly used chemotherapy treatment for prostate cancer.[18] Detecting early responses is crucial to ensure effective treatment. Based on detection, a non-effective treatment can be changed to another one in the early phase. MRI offers a non-invasive way of detecting treatment responses with various contrasts.

The driving hypothesis of the current work was that rotating frame relaxation times T_{RAFF2} and T_{RAFF4} pick up docetaxel chemotherapy response earlier than the continuous wave $T_{1\rho}$, adiabatic $T_{1\rho}$ and adiabatic $T_{2\rho}$ in subcutaneous red fluorescent protein transfected prostate cancer

(PC3-RFP) tumors in mice. The rotating frame relaxation time results were compared and correlated with current standard methodologies, including the water apparent diffusion coefficient (ADC), T_1 and T_2. Furthermore, the tumor response to docetaxel chemotherapy was verified by estimating the tumor volume on T_2-weighted images, as well as using histology and optical imaging.

2 | MATERIALS AND METHODS

2.1 | Animals and chemotherapy

Human prostate cancer cells expressing red fluorescence protein (PC3-RFP, Anticancer, San Diego, CA) were implanted subcutaneously in the right hind limbs of 21 nude male mice (athymic nude—Foxn1[nu], Harlan, Frederick, MD). The mice had ad libitum access to water and food during the experiment period. The mice were divided into control (n = 11) and treatment (n = 10) groups. The tumor growth and treatment responses were monitored once a week for 4 weeks using optical imaging and MRI. For the treatment group, 15 mg/kg of docetaxel Actavis (2 mg/ml)[19] chemotherapy (Kuopio University Hospital pharmacy) was administered intraperitoneally once a week starting after imaging in Week 1 from the tumor cell implantation. All the experiments were conducted with approval from the Animal Experiment Board in Finland and conducted in accordance with the guidelines set by the European Commission Directive 2010/63/EU.

2.2 | MRI

All the MRI experiments were carried out using a PharmaScan 7 T magnet (Bruker, Ettlingen, Germany) equipped with a 71 mm volume transmitter and a 20 mm single loop receiver coil. For imaging, the animals were anesthetized using 4% isoflurane in 30% O_2 and 70% N_2 for induction, and the isoflurane level was reduced to 1.5% to maintain anesthesia during imaging. Multislice T_2-weighted images (time-to-repetition (TR) = 2500 ms, effective echo time (TE) = 33 ms, echo train length 8, matrix size 256 × 256, field-of-view = 30 × 30 cm^2 and 15 slices with slice thickness of 1 mm) were acquired to measure the tumor volume and to locate an axial slice with the largest cross-sectional tumor area for further measurements. To measure the RAFFn relaxation times, T_{RAFF2} and T_{RAFF4}, magnetization was prepared using 0, 9, 18 and 36 ms pulse trains consisting of RAFF in the second rotating frame (RAFF2) or fourth rotating frame (RAFF4) pulses with an RF power of $\gamma B_1/(2\pi)$ = 1250 Hz for RAFF2 and 648 Hz for RAFF4. When the RF waveforms were reconstructed, a power of 1250 Hz was used, resulting in a 1.13 ms RAFF2 pulse duration to maintain a 45° angle between the magnetization and the final effective field, similar to earlier studies.[12,17] The RAFFn relaxation measurements were repeated with an initial inversion to assess the formation of a steady signal state during RAFF2 and RAFF4 irradiation.[12] The total duration of RAFF2 and RAFF4 measurements was 6 min 24 s each, taking into account scans with and without initial inversion. The continuous wave $T_{1\rho}$ spin-lock times were 0, 9, 27 and 45 ms with an RF power of $\gamma B_1/(2\pi)$ = 1250 Hz. Adiabatic half passages with a pulse duration of 6 ms and $\gamma B_1/(2\pi)$ = 1250 Hz were applied for excitation and returning magnetization in the B_0 direction.[20] For adiabatic $T_{1\rho}$ ($T_{1\rho,adiab}$), magnetization was prepared using 0, 18, 36 and 72 ms long pulse trains consisting of full passage adiabatic hyperbolic secant pulses with pulse durations of 4.525 ms to match the RAFF2 and RAFF4 pulses and a peak RF power of 2100 Hz. Similar pulse trains were applied between two adiabatic half passage pulses (pulse duration 3 ms and $\gamma B_1/(2\pi)$ = 1700 Hz) to measure the adiabatic $T_{2\rho}$ ($T_{2\rho,adiab}$). The conventional T_2 was measured using an adiabatic Hahn double echo preparation with TE = 8, 17, 26, 64 ms, and T_1 with saturation recovery and TE = 200, 600, 1500, 5000 ms. To measure B_1, the data were acquired using a hard pulse with a nominal RF power of 625 Hz to prepare the magnetization, incrementing the hard pulse duration in eight steps 0.2 ms at a time from 0 ms to 1.4 ms.[21] The acquisition time for continuous wave $T_{1\rho}$, $T_{1\rho,adiab}$, $T_{2\rho,adiab}$, T_2, T_1 and B_1 measurements was 3 min 12 s for each. An identical fast spin echo readout sequence with fat suppression was applied for all the relaxation time measurements (TR = 4000 ms, effective TE = 8 ms, echo train length = 8, field of view = 30 × 15 mm^2, matrix size 256 × 128, and slice thickness 1 mm). The B_1 data were acquired with a smaller matrix size of 128 × 64. The water ADC was estimated from the data measured with two sets of b values; low values of b = 0, 2, 4, 6, 9, 12, 14, 18, 23, 25, 28, 50, 100, 300, 500 s/mm^2 and high values of b = 0, 100, 300, 500, 700, 900, 1100, 1300, 1500, 1700, 1900, 2000 s/mm^2 in a spin-echo echo planar imaging sequence (TR = 3750 ms, TE = 25 ms for low b-values, TR = 3000 ms, TE = 30 ms for high b values, matrix size 128 × 64, field-of-view = 30 × 15 mm^2 and slice thickness 1 mm). The acquisition time for the low b-value set was 22 min 30 s and for the high b-value set 14 min 24 s. The total scanning time for each animal was around 1 h 30 min with all the shimming and calibrations included.

2.3 | Optical imaging

Tumor cells contained a red luciferase gene, which allowed optical imaging of the tumors during the experimental period. On the day following the MRI, the mice were anesthetized for optical imaging with isoflurane similarly as for MRI and imaged in an IVIS Lumina II optical imaging device

(Perkin Elmer, Waltham, MA). We placed two to four mice simultaneously in the optical imaging chamber. The mice were placed on the left flank since the tumors were located in the right hind leg under the skin. Then the imaging was performed with the following parameters: exposure time auto/1 s, binning medium, f-stop 2, excitation filter 535 and 465 (background) and emission filter DsRed. The tumor volume was quantified by integrating the red-light signal over the tumor area.

2.4 | Histology

After a four-week treatment or control period, the animals were euthanized with an isoflurane overdose and the right hind limbs with the tumors were fixed using 10% formalin. After fixation, the tumors together with calf muscle were removed from the limbs, and the tissue was embedded in paraffin. The tumors were cut into 4 μm thick sections, and sections from the MRI slice volume were mounted on glass and stained with hematoxylin and eosin to study the cytoarchitecture of the treated and control tumors. A histological examination of the tumors and photomicrographs was carried out using an Axio Imager 2 microscope (ZEISS, Jena, Germany).

2.5 | Data and statistical analysis

Relaxation time maps were calculated in a pixel-by-pixel manner using AEDES software (http://aedes.uef.fi) on the MATLAB platform (MathWorks, Natick, MA). RAFFn data with and without initial inversion were fitted with a model taking the steady state into account by using monoexponential rise and decay functions to the same steady state value,[12] and a linear fit was applied for the log transform of $T_{1\rho}$, T_2 and water ADC. A cosine function to estimate the RF pulse power was fitted for the B_1 data. The relaxation time, water ADC and B_1 parameters were averaged over hand-drawn regions of interest (ROIs) representing the tumor based on the T_2-weighted images. The tumor volumes were determined using the hand-drawn ROIs over T_2-weighted anatomical images covering the whole tumor in three dimensions. All the data are reported as mean ± standard deviation.

A two-way repeated measures analysis of variance (ANOVA) with a Bonferroni post-test was applied to compare the relaxation times and ADC as a function of time in the treated versus the control group. This was also used to compare the tumor volumes between the treated and control group determined by optical imaging. The significance of the differences between time points was calculated using a Student's t test, and Benjamini-Hochberg false discovery rate (FDR) correction[22] was used to correct for multiple comparisons. The temporal changes in the tumor volume within groups determined from T_2-weighted images were analyzed using a one-way repeated measures ANOVA with Bonferroni post-test. The Pearson correlation was calculated in order to evaluate the association between the RAFFn and ADC values. A p-value less than 0.05 was considered significant.

2.6 | Data availability statement

The data that support the findings of this study are available from the corresponding author upon reasonable request.

3 | RESULTS

3.1 | Decreased tumor volume in the treated group

The first injection of the docetaxel chemotherapy was given 1 week after the implantation of the PC3-RFP tumor cells into the animals in the treatment group. The tumors displayed hyperintensity in the T_2-weighted images with clear tumor edges (Figures 1A and 1B). The tumor volumes in both the treated and control groups were equal before treatment as verified in the T_2-weighted MRI taken at the first week time point (19.26 ± 13.12 mm^3 versus 18.47 ± 11.35 mm^3, $P = 0.89$, Figures 1C and 1D). In the treated group, all the tumor volumes had decreased between the first (19.25 ± 13.12 mm^3) and fourth (7.64 ± 6.72 mm^3, $P < 0.001$) weeks (Figure 1C), whereas the tumor volumes had clearly increased from 18.47 ± 11.35 mm^3 to 317.80 ± 269.81 mm^3 ($P < 0.001$) in the control group (Figure 1D). The treated group showed a clear reduction in the tumor volume at the four-week time point; however, the cell density varied within the tumor and between animals. Two cases showed just scattered potential tumor cells in the tissue. Another two animals showed widespread highly dense but small focuses of potential tumor cells. The rest of the animals still exhibited a proper tumor with highly dense areas with small cells, necrotic cores and/or areas with tumor tissue as in the controls (Figure 1E). Figure 1E shows a representative example of a tumor with these three morphological features. The tumors in the control group were highly dense, except for necrotic areas mainly in the center of the tumor (Figure 1F).
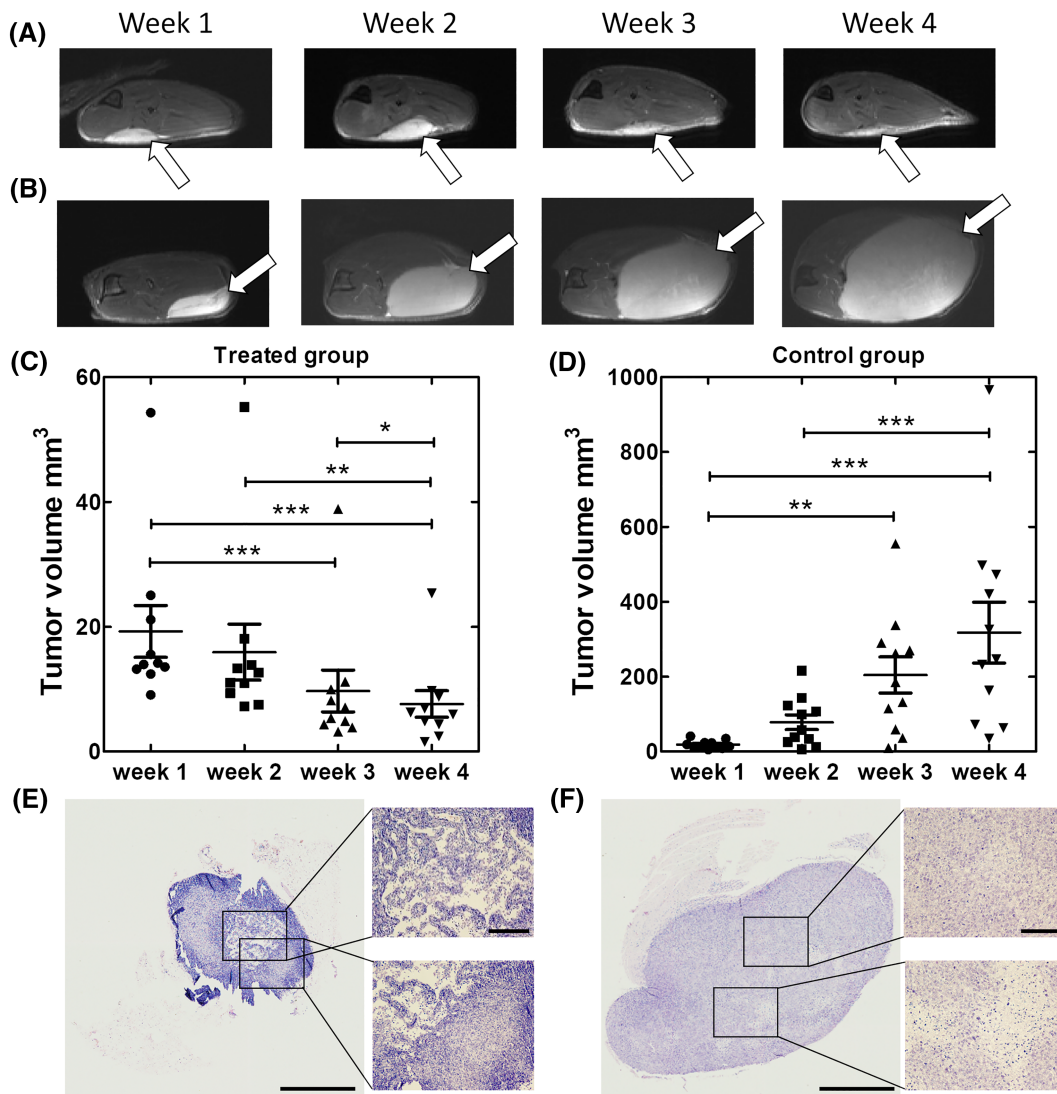
FIGURE 1 Evolution of tumor volume observed in the MR imaging slice. A, B, T_2-weighted MR images of a treated tumor (A) compared with a control tumor (B). The white arrows with a black outline in A and B point to the tumors. C, D, Tumor volumes based on T_2-weighted MR images from treated group (C) and control group (D). E, F, Hematoxylin- and eosin-stained sections at a four-week time point for treated (E) and control (F) groups. The scale bar in E and F is 2300 μm in the full images and 156 μm in the close-up images. One-way repeated measures ANOVA with Bonferroni post-test was performed to assess the difference between time points (*$P < 0.05$, **$P < 0.01$, ***$P < 0.001$)

3.2 | Decreased relaxation times in the treated group

All the relaxation times (T_{RAFF2}, T_{RAFF4}, $T_{1\rho}$, $T_{1\rho,adiab}$, $T_{2\rho,adiab}$, T_1 and T_2) decreased in the treated group compared with the control group during the treatment period (Figure 2). This was seen as a significant difference in the trends between the treated and control groups. For instance, the T_{RAFF2} values decreased from the first week (111 ± 15 ms) to the fourth week (81 ± 7 ms) in the treated group ($P < 0.001$) and from 122 ± 18 ms to 109 ± 4 ms in the control group ($P = 0.22$). Similarly, the T_{RAFF4} values decreased from 361 ± 49 ms to 282 ± 32 ms in the treated group ($P = 0.004$) and from 403 ± 36 ms to 390 ± 14 ms in the control group ($P = 0.83$) (Figure 2). There were also significant differences between the groups at the three- and four-week time points (Figure 2). When comparing the timepoints with the before treatment values, the earliest treatment responses were found with T_{RAFF2}, $T_{1\rho,adiab}$, $T_{2\rho,adiab}$, T_1 and T_2 at the two-week time point, ie after 1 week of treatment. The clearest short- and long-term responses were obtained with T_1 (Figure 2). Overall, in all the relaxation time curves over time, a similar decreasing trend was present. The baseline (Week 1) T_{RAFF4} and $T_{1\rho,adiab}$ values in the treated and control groups were different ($P < 0.05$). Histograms of the T_2 and RAFF2 measurements in tumor areas for both groups are shown in Figure 3. Both T_2 and RAFF2 histograms were able to discriminate the treated tumor tissue from the control tumors, with T_2 showing a clearer difference.
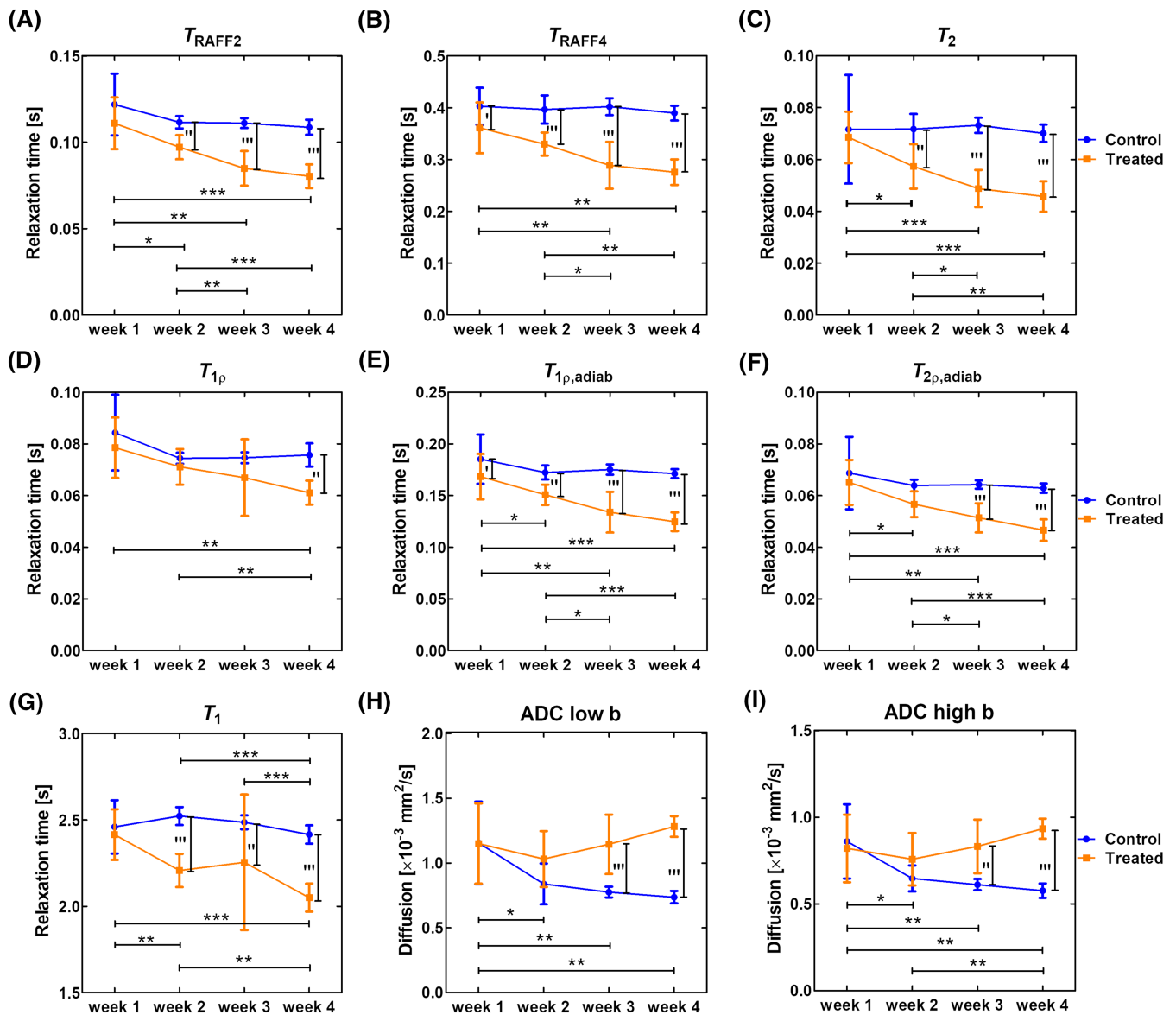
FIGURE 2 Average relaxation times and water diffusion from control group and treated group during the four-week study period: A, T_{RAFF2}; B, T_{RAFF4}; C, T_2; D, $T_{1\rho}$; E, adiabatic $T_{1\rho}$; F, adiabatic $T_{2\rho}$; G, T_1; H, water ADC obtained with low b values, and I, water ADC obtained with high b values. The interaction between trends and the comparisons between the groups were done using a two-way repeated measures ANOVA and Bonferroni post-test ($'P < 0.05$, $''P < 0.01$, $'''P < 0.001$). All the interactions between trends, except the continuous wave $T_{1\rho}$, were significant. The significance between the time points was then calculated using Student's t test and the results were corrected with a Benjamini-Hochberg FDR correction for multiple comparisons ($*P_{FDR} < 0.05$, $**P_{FDR} < 0.01$, $***P_{FDR} < 0.001$)

3.3 | Increased water ADC in the treated group

An increasing trend in the water ADC during the treatment was observed in the treated group with both low and high b values. The water ADC increased from Week 1 ($115 \pm 31 \times 10^{-5}$ mm^2/s) to Week 4 ($127 \pm 20 \times 10^{-5}$ mm^2/s), $P = 0.41$, and from Week 1 ($80 \pm 19 \times 10^{-5}$ mm^2/s) to Week 4 ($90 \pm 15 \times 10^{-5}$ mm^2/s), $P = 0.40$, when the low and high b-value datasets were considered, respectively. In the control group, a significant decrease was observed with low b values from Week 1 ($116 \pm 32 \times 10^{-5}$ mm^2/s) to Week 4 ($74 \pm 5 \times 10^{-5}$ mm^2/s), $P = 0.008$, and with high b values from Week 1 ($86 \pm 21 \times 10^{-5}$ mm^2/s) to Week 4 ($58 \pm 41 \times 10^{-5}$ mm^2/s), $P = 0.008$. These opposite trends led to significantly larger water ADC values in the treated group compared with the control group at the three- and four-week time points (Figure 2). The increased water ADCs of the treated tumors are supported by the reduced cell density seen in the histology (Figure 2). Higher water ADCs were found when using low compared with high b values. When evaluating the association between the T_{RAFF2} or T_{RAFF4} values and the water ADC, there was a strong
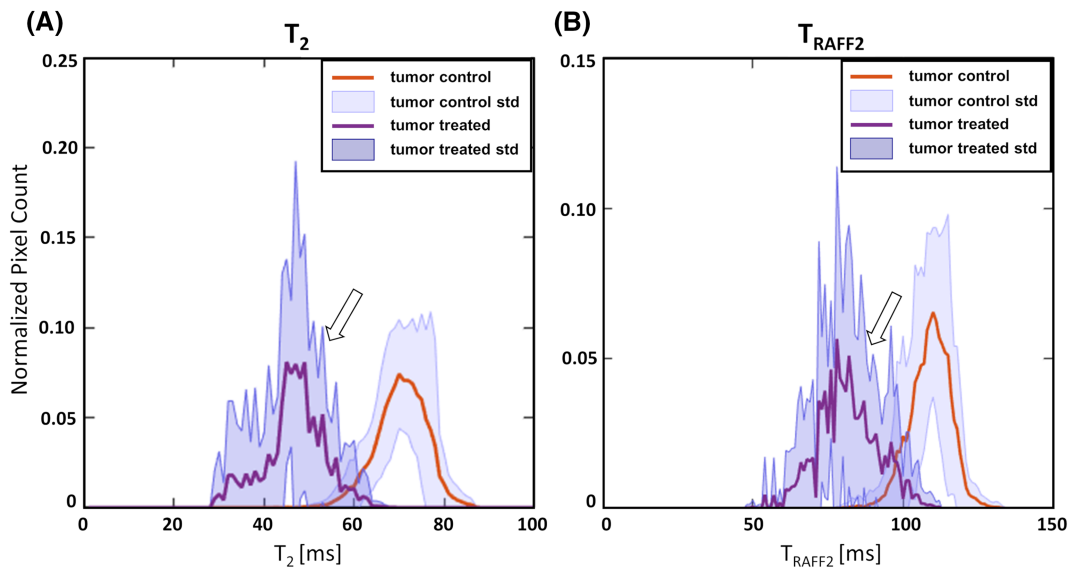
FIGURE 3 Histograms from all T_2 (A) and RAFF2 (B) measurements versus a normalized pixel count of the tumor areas in the control and treated groups. The arrows point to the treated tumor peaks. The treated tumor peak was clearly isolated from the control group tumor peaks in both measurements

association between T_{RAFF2} and ADC with low b values ($R^2 = 0.69$, $P < 0.001$) and ADC with high b-values ($R^2 = 0.76$, $P < 0.001$) in the control group (Supplementary Table S1). There was also a significant but weak correlation between T_{RAFF4} and ADC with low b values ($R^2 = 0.11$, $P < 0.05$) and ADC with high b values ($R^2 = 0.16$, $P < 0.01$) in the control group. No associations were found in the treated group ($R^2 < 0.01$) (Supplementary Table S2).

3.4 | No temporal alterations in RAFF2 and RAFF4 steady state signals

Furthermore, we analyzed the steady state from the RAFFn relaxation data. In Week 1 the initial RAFF2 steady state average values were 0.14 ± 0.02 for the treated group and 0.15 ± 0.02 for the control group (Figure 4A). For the RAFF4 values in Week 1, the steady state was 0.60 ± 0.05 in the treated group and 0.66 ± 0.09 in the control group (Figure 4B). The steady state remained stable during the four-week experimental period (0.12 ± 0.01 for treated RAFF2 and 0.14 ± 0.01 for control RAFF2, 0.62 ± 0.08 in treated RAFF4 and 0.61 ± 0.03 in control RAFF4; Figures 4A and 4B). The RAFF4 data exhibited a noisier steady state map than the RAFF2 data, which also led to weaker contrast between tumor and intact muscle tissue (Figures 4C and 4D).

3.5 | RAFFn contrast and B_1

RAFFn contrast is created by applying amplitude- and frequency-modulated RF irradiation (B_1). To analyze the variation of the RAFFn relaxation times in terms of B_1 heterogeneity, the RAFF2 and RAFF4 relaxation time maps together with the B_1 map from a representative control tumor are shown where the largest B_1 variation was present among both groups (Figure 5). It is notable that RAFFn variation within this B_1 range is minimal and the spatial T_{RAFFn} variation originates from anatomic-related sources.

3.6 | Optical imaging

To monitor the chemotherapy responses, the optical imaging of RFP activity from viable tumor cells was imaged. The photon count trend decreased gradually from the beginning (490 ± 300) to the end of the four-week imaging period (290 ± 220) in the treated group. The photon count intensity increased from the beginning (660 ± 220) to the end of the four-week imaging period (1480 ± 850, $P = 0.001$) in the control group, indicating an increased number of viable tumor cells and tumor growth leading to increased expression of RFP-related red light (Figure 6).
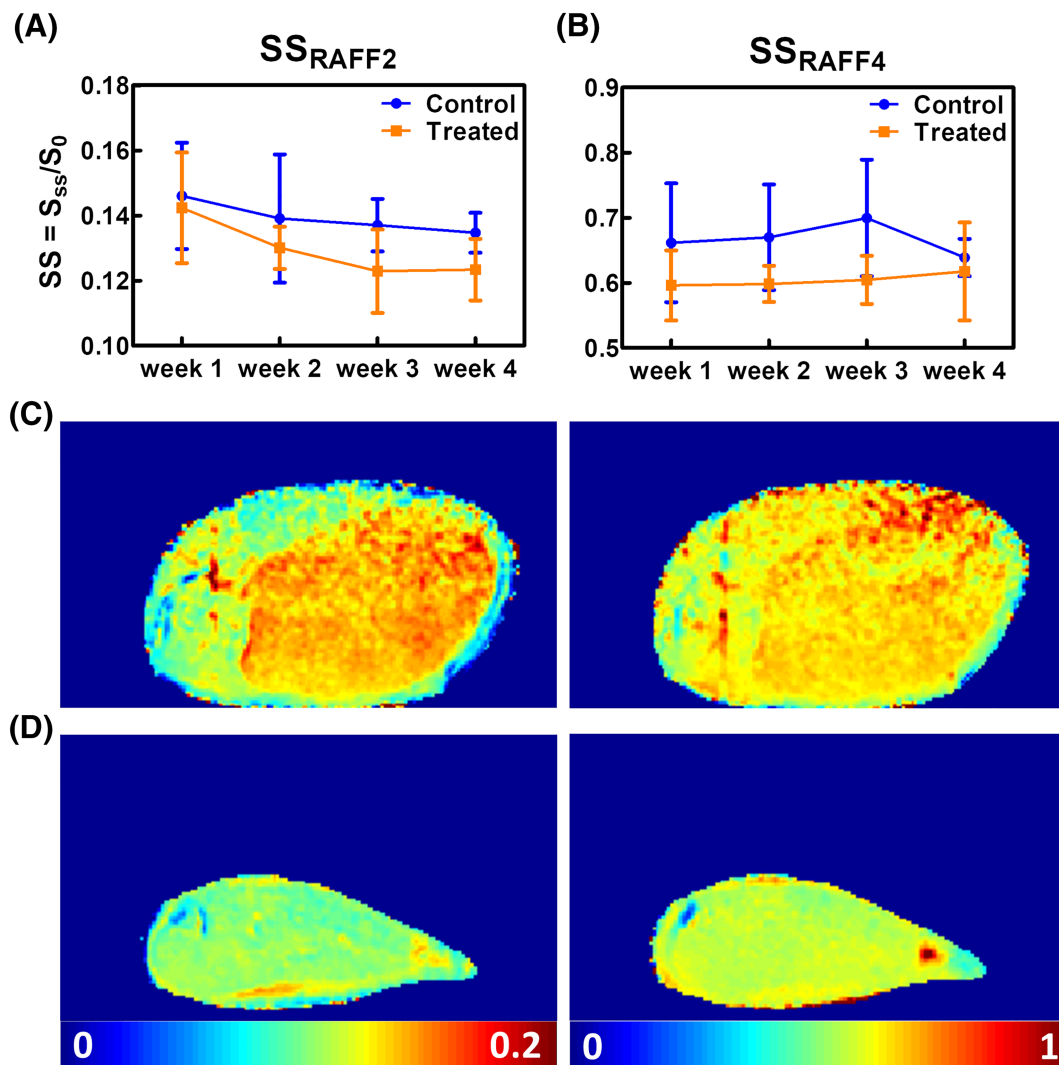
FIGURE 4 A, B, RAFF2 (A) and RAFF4 (B) steady state evolution from a tumor slice with the largest tumor from control and treated groups during the four-week study period. C, D, Examples of the RAFFn steady state maps of the control group (C) and the treated group (D). Comparisons between the groups were done using a two-way repeated measures ANOVA without significant differences
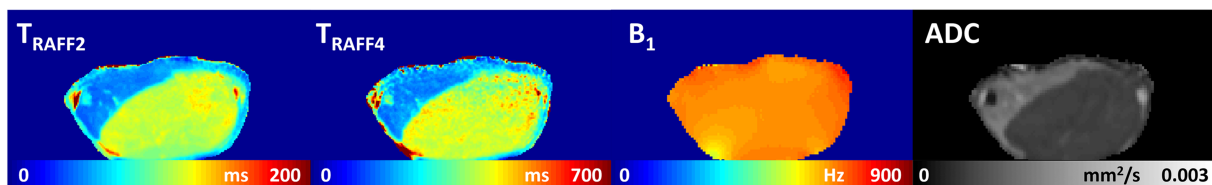

FIGURE 5 Example of the RAFFn relaxation time maps and corresponding B_1 and a water ADC map from a measurement with low b values from one control mouse in Week 4

3.7 | Associations between parameters

Correlations between the different measures obtained were calculated in order to examine their associations. In the control group, all the relaxation times had strong correlations with one another (Supplementary Table S1). No correlation was found between the relaxation times and optical imaging measures or tumor volume in the control group. The tumor volume defined from T_2-weighted images correlated strongly with the tumor volume obtained from optical imaging in the control group ($r = 0.87$). In the treated group the relaxation times exhibited again strong correlations, but they did not correlate with the ADC values. Correlations between the optical imaging measures and relaxation times were also weak in the

FIGURE 6 A, B, Optical images of treated (A) and control (B) mice at one-, two-, three- and four-week time points. C, Photon counts integrated over the tumor areas in treated and control groups. Comparisons were done using a two-way repeated measures ANOVA with a Bonferroni post-test ($''P < 0.01$, $'''P < 0.001$)
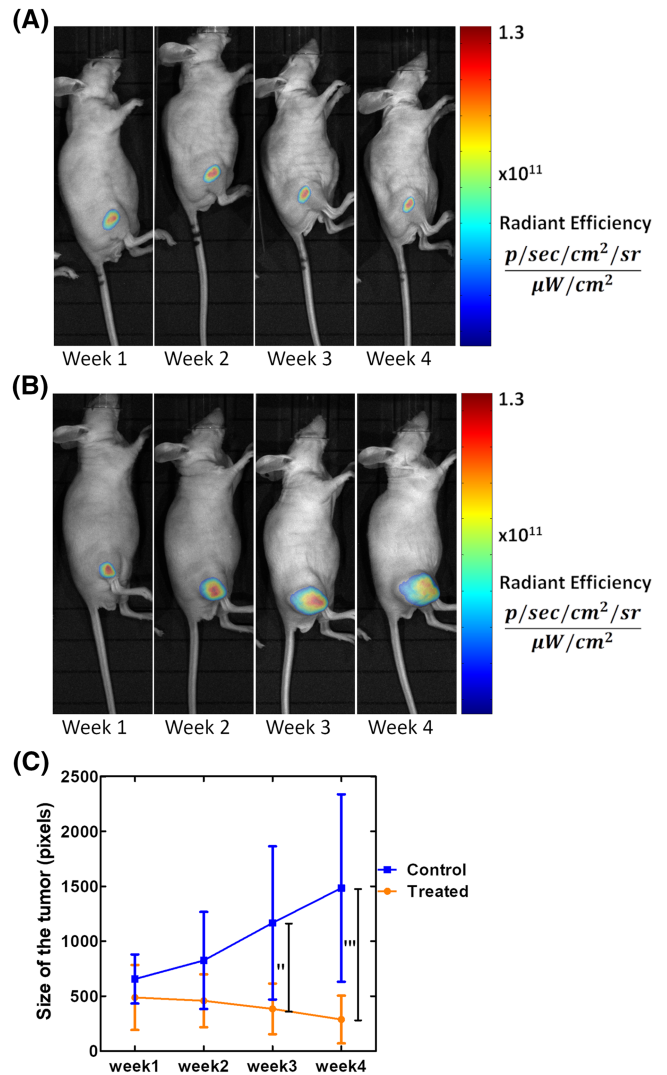
treated group. Only the T_1 and T_2 values had a moderate correlation ($r > 0.4$) with the tumor volume determined from the T_2-weighted images (Supplementary Table S2). Tumor volumes defined from T_2-weighted images and optical images did not correlate in the treated group.

4 | DISCUSSION

The treatment response of docetaxel chemotherapy on prostate tumors of nude mice was evaluated by using several magnetic resonance relaxation times and water ADC. All relaxation times exhibited a decrease as a response to chemotherapy in the treated group while the relaxation times in the control group remained stable. ADCs of the treated group showed an increasing trend during the treatment in comparison with the decrease seen in the control group. The tumor volumes in the treated group decreased gradually while in the control group tumor volumes increased with close to exponential growth. Optical imaging and histology supported the MRI findings.

All relaxation times excluding continuous wave $T_{1\rho}$ values showed a difference in trends between treated and non-treated mice. Visually similar differences were observed with continuous wave $T_{1\rho}$ values as well, but with smaller differences between the curves. Furthermore, the relaxation times decreased in the treated group, indicating a response to the therapy. The histological tumor size decreased in the treated group compared with the control group, although the heterogeneity of the cell density was large within the treated tumors. Increased relaxation times have been associated with positive anticancer treatment and decreased cell density in several animal anti-cancer treatment models. In a rat intracranial glioma model, a large increase of T_{RAFF2} and $T_{1\rho}$ relaxation times was found simultaneously with reduced tumor sizes and cell density.[13]

Our results showed decreasing T_1 values as a response to chemotherapy. Similar results have been reported using patupilone, 5-fluorouracil, paclitaxel, everolimus and vatalanib treatments in fibrosarcoma, melanoma and mammary tumors, and cervical cancer mouse tumor models.[23] In

an RIF-1 fibrosarcoma model treated successfully with patupilone, reduced T_1 values and increased water ADCs were reported,[23] thus supporting our findings. Additionally, in the same model, an increased composite parameter for permeability and interstitial space derived from a contrast agent perfusion experiment indicated increased extracellular space and/or permeability according to the authors.[23] Our histology supports increased extracellular space in our study; however, this is expected to lead to increased T_2 values, which were not observed. Instead, a decrease in the T_2 values as well as in the other relaxation times was found. A similar T_2 value decrease and increase in the water ADC were reported by Schreurs et al in subcutaneous colon carcinoma tumors undergoing photodynamic treatment.[24] In addition to the T_1 and T_2 values, the rotating frame relaxation times also decreased during the docetaxel treatment. Previously, an increase of these relaxation times has been associated with successful therapy, which is opposite to our findings. Duvvuri et al studied continuous wave $T_{1\rho}$ values in a murine radiation-induced fibrosarcoma model undergoing cyclophosphamide treatment.[25] Increased continuous wave $T_{1\rho}$,[7,8] T_1 and T_2 values, spin density and water ADC[7] were associated with positive gene therapy outcome in a rat herpes simplex virus thymidine kinase gene-transfected BT4C glioma model treated with ganciclovir. Similarly, increased adiabatic $T_{1\rho}$ and $T_{2\rho}$ values[11,13] as well as T_{RAFF2} values[13] were associated with positive treatment outcomes in the same animal model. These studies represent both subcutaneous and intracranial tumors with consistent treatment outcomes. The discrepancies between our relaxation time results and the previous findings underline the importance of knowing the tumor type that is imaged as well as taking into account the therapy type and dose used. The therapy outcome may represent itself in either decreased or increased relaxation times depending on the tumor tissue together with the treatment type. Furthermore, here in the case of PC3 prostate cancer with docetaxel chemotherapy, no clear difference between the rotating frame methods and traditional relaxation times was seen; instead, they all showed similar decreases as a response to the treatment.

In this study, the water ADC had a trend up in the treated group and decreased significantly in the control group compared with the first time point, ending up in significant differences between the groups at the three- and four-week time points. A previous study using the PC3 cell line with docetaxel (40 mg/kg/week) chemotherapy resulted in a 30% increase in the water ADC 14 days after starting the chemotherapy.[26]

We did not find a clear increase and the discrepancy is most likely due to the almost three times higher docetaxel dose in the previous study compared with ours (15 mg/kg/week). The initial ADCs agreed well between our and the previous study (90×10^{-5} mm^2/s).[26]

Water diffusion measurements may lead to increased or decreased water ADC as a response to therapy.[13,27,28] With a lower docetaxel dose, however, the tumor size remained constant without any significant increase in the water ADC. The low dose may also affect the relaxation times, which decreased compared with those of the control tumors. A change in the relaxation mechanisms, including less ^{1}H exchange, may contribute in an opposite manner to increased extracellular space, which is typically the main contributor to increased T_2 values and water ADC in anticancer treatments. Within the tumor, no association between T_{RAFF2} or T_{RAFF4} relaxation times and the water ADC was found either for low or high b values in the treated group ($R^2 < 0.01$). This is opposite to what was reported in a herpes simplex thymidine kinase gene-transfected rat glioma BT4C model undergoing ganciclovir treatment, where a positive correlation between the T_{RAFF2} relaxation time and water ADC was reported.[13] Based on the difference, opposite mechanisms of increased water mobility due to increased extracellular space and cell death are associated with the decreased relaxation times.

Steady state formation during RAFFn irradiation has been introduced as one image contrast.[12] Previously, a clear contrast between white and grey matter was found with steady state and RAFFn relaxation times.[29] This is, to our best knowledge, the first time that steady state maps have been presented from tumors. The steady state contrast between control and treated tumors was found to be weak without a significant response to chemotherapy, indicating less efficient performance as a treatment marker than relaxation times. Since this is the first study in one cell line with one treatment model, the evaluation of the steady state as a marker for anti-cancer treatment may be continued.

The tumor volume in the treated group decreased, indicating cell death and successful anti-cancer treatment. This is supported by the histology, where a visual inspection indicated spatially variable cell density 4 weeks after the tumor implantation, while the cell density was high and more homogeneous in the control group. As a response to the treatment, an immune cell infiltration is expected to take place and macrophages are clearing the necrotic cells from the treated tumors. Thus, inflammation as a treatment response may be present in the treated group. A homogeneous signal intensity was present in the T_2-weighted images, indicating minor vascular necrosis in the tumor core in both treated and non-treated tumors. Interestingly, the T_2 and RAFF2 values of the treated tumors were clearly different from the control group tumor values when looking at the histograms. In both T_2 and RAFF2, the control tumors exhibited longer relaxation times than the treated tumors. Previously, RAFF2 was found to correlate with tumor cell density in a rat glioma study better than other studied relaxation times, including T_2.[13] Here, however, T_2 appeared to show the difference between treated and control tumors even more clearly than RAFF2.

Overall, our hypothesis was that the RAFFn method would pick up the therapy responses earlier or more specifically than the traditional methods. Previously RAFF2 was shown to correlate the best with the cell density in all the glioma tumor areas when comparing with other studied relaxation times.[13] In that study, the glioma tumors were divided into core, intermediate and periphery areas and represented clear regional cell densities. In our case, however, the tumor tissue was more homogeneous and did not reveal such differences between the methods, and similar regional analysis would have not given any further information. Thus, in this case of a prostate cancer mouse model, the different methods did not differ as much as we expected. This result underlines the importance of choosing the detection method according to the target and its physicochemical properties. These properties may include changes in cell density, extracellular space, specific metabolites and blood flow among many others, which then can be exploited to optimize MRI parameters.

The RAFFn method, as is any rotating frame method, is dependent on the applied B_1 field. The method was found to be relatively insensitive to B_0 inhomogeneities because of the refocusing nature of the RAFF pulses. The method is still sensitive to B_1 inhomogeneities and thus the B_1 field was measured to confirm that the observed result was arising from biological changes and not from B_1 field inhomogeneity. Our results demonstrated that the B_1 field was homogeneous throughout the tumor and muscle, making the results reliable. The dependence on the applied B_1 field may, however, be an issue in clinical prostate imaging settings with larger targets and the location of the tumors. The feasibility of using the RAFF2 method in clinical prostate cancer imaging at 3 T has been demonstrated previously,[14,16] and furthermore T_{RAFF2} was shown to be highly repeatable in that setting.[16]

Due to the small size of the tumors at the four-week time point in the treated group, the relaxation time mapping and ADC measurements may suffer from partial volume effects from surrounding edema fluid. However, the relaxation times gradually decreased in the treated group from week to week, indicating minor effects from the partial volume. The heterogeneity of the tumor tissue or differences in the treatment response may contribute to the larger standard deviation at the three-week time point. The tumor ROIs covered the whole tumor and the possible minor necrotic, as well as more dense, areas were included. The increased relaxation times are expected on necrotic areas. Only few small spots of increased relaxation times were detected, which have negligible effect on tumor mean relaxation times. The treated tumors were small at every time point, which precluded differentiation of the necrotic areas from the relaxation time maps. Overall, the areas showing increased or decreased relaxation times within the ROIs mostly increase the standard deviation of the values, and avoiding them would not change the relaxation times significantly.

5 | CONCLUSIONS

Decreased relaxation times as a result of successful chemotherapy were observed. There were non-significant differences in treatment response detection of PC3 prostate cancer docetaxel treatment with applied relaxation times. The results indicate that altered relaxation mechanisms are taking place with the used treatment as compared with higher dose chemotherapies applied earlier. It is evident from this work that tumor type and treatment dosage can greatly impact biomarker evaluation.

ORCID

Hanne Laakso https://orcid.org/0000-0003-1142-9008
Ivan Jambor https://orcid.org/0000-0001-6305-3570
Timo Liimatainen https://orcid.org/0000-0001-7472-9900

REFERENCES

1. Engholm G, Ferlay J, Christensen N, et al. *Cancer Incidence, Mortality, Prevalence and Survival in the Nordic Countries*. Association of the Nordic Cancer Registries. Danish Cancer Society; 2019. http://www.ancr.nu
2. Woodrum DA, Kawashima A, Gorny KR, Mynderse LA. Prostate cancer: state of the art imaging and focal treatment. *Clin Radiol*. 2017;72(8): 665-679.
3. Marko J, Gould CF, Bonavia GH, Wolfman DJ. State-of-the-art imaging of prostate cancer. *Urol Oncol*. 2016;34(3):134-146.
4. Jambor I. Optimization of prostate MRI acquisition and post-processing protocol: a pictorial review with access to acquisition protocols. *Acta Radiol Open*. 2017;6(12):2058460117745574. https://doi.org/10.1177/2058460117745574
5. Ahmed H, Kirkham A, Arya M, et al. Is it time to consider a role for MRI before prostate biopsy? *Nat Rev Clin Oncol*. 2009;6(4):197-206.
6. Valerio M, Donaldson I, Emberton M, et al. Detection of clinically significant prostate cancer using magnetic resonance imaging-ultrasound fusion targeted biopsy: a systematic review. *Eur Urol*. 2015;68(1):8-19.
7. Hakumäki JM, Gröhn OH, Tyynelä K, Valonen P, Ylä-Herttuala S, Kauppinen RA. Early gene therapy-induced apoptotic response in BT4C gliomas by magnetic resonance relaxation contrast T_1 in the rotating frame. *Cancer Gene Ther*. 2002;9(4):338-345.
8. Kettunen MI, Sierra A, Närväinen MJ, et al. Low spin-lock field T1 relaxation in the rotating frame as a sensitive MR imaging marker for gene therapy treatment response in rat glioma. *Radiology*. 2007;243(3):796-803.
9. Michaeli S, Sorce D, Springer C, Ugurbil K, Garwood M. $T_{1\rho}$ MRI contrast in the human brain: modulation of the longitudinal rotating frame relaxation shutter-speed during an adiabatic RF pulse. *J Magn Reson*. 2006;181:138-150.
10. Michaeli S, Sorce DJ, Idiyatullin D, Ugurbil K, Garwood M. Transverse relaxation in the rotating frame induced by chemical exchange. *J Magn Reson*. 2004;169(2):293-299.
11. Sierra A, Michaeli S, Niskanen JP, et al. Water spin dynamics during apoptotic cell death in glioma gene therapy probed by $T_{1\rho}$ and $T_{2\rho}$. *Magn Reson Med*. 2008;59(6):1311-1319.
12. Liimatainen T, Sorce DJ, Connell R, Garwood M, Michaeli S. MRI contrast from relaxation along a fictitious field (RAFF). *Magn Reson Med*. 2010;64(4): 983-994.

13. Liimatainen T, Sierra A, Hanson T, et al. Glioma cell density in a rat gene therapy model gauged by water relaxation rate along a fictitious magnetic field. *Magn Reson Med*. 2012;67(1):269-277.

14. Jambor I, Pesola M, Merisaari H, et al. Relaxation along fictitious field, diffusion-weighted imaging, and T_2 mapping of prostate cancer: prediction of cancer aggressiveness. *Magn Reson Med*. 2016;75(5):2130-2140.

15. Epstein JI, Egevad L, Amin MB, et al. The 2014 International Society of Urological Pathology (ISUP) Consensus Conference on Gleason Grading of Prostatic Carcinoma: definition of grading patterns and proposal for a new grading system. *Am J Surg Pathol*. 2016;40(2):244-252.

16. Jambor I, Pesola M, Taimen P, et al. Rotating frame relaxation imaging of prostate cancer: repeatability, cancer detection, and Gleason score prediction. *Magn Reson Med*. 2016;75(1):337-344.

17. Liimatainen T, Hakkarainen H, Mangia S, et al. MRI contrasts in high rank rotating frames. *Magn Reson Med*. 2015;73(1):254-262.

18. Pagliuca M, Buonerba C, Fizazi K, Di Lorenzo G. The evolving systemic treatment landscape for patients with advanced prostate cancer. *Drugs*. 2019; 79(4):381-400.

19. Johnson CV, Shelton T, Smith CJ, et al. Evaluation of Combined ^{177}Lu-DOTA-8-AOC-BBN (7-14)NH$_2$ GRP receptor-targeted radiotherapy and chemotherapy in PC-3 human prostate tumor cell xenografted SCID mice. *Cancer Biother Radiopharm*. 2006;21(2):155-166.

20. Gröhn OH, Kettunen MI, Mäkelä HI, et al. Early detection of irreversible cerebral ischemia in the rat using dispersion of the MRI relaxation time, $T_{1\rho}$. *J Cereb Blood Flow Metab*. 2000;20(10):1457-1466.

21. Vaughan JT, Adriany G, Garwood M, et al. Detunable transverse electromagnetic (TEM) volume coil for high-field NMR. *Magn Reson Med*. 2002;47(5): 990-1000.

22. Benjamini Y, Hochberg Y. Controlling the false discovery rate: a practical and powerful approach to multiple testing. *J R Stat Soc B*. 1995;57(1): 289-300.

23. McSheehy PM, Weidensteiner C, Cannet C, et al. Quantified tumor T_1 is a generic early-response imaging biomarker for chemotherapy reflecting cell viability. *Clin Cancer Res*. 2010;16(1):212-225.

24. Schreurs TJ, Hectors SJ, Jacobs I, Grull H, Nicolay K, Strijkers GJ. Quantitative multi-parametric magnetic resonance imaging of tumor response to photodynamic therapy. *PLoS ONE*. 2016;11(11):e0165759. https://doi.org/10.1371/journal.pone.0165759

25. Duvvuri U, Poptani H, Feldman M, et al. Quantitative $T_{1\rho}$ magnetic resonance imaging of RIF-1 tumors in vivo: detection of early response to cyclophosphamide therapy. *Cancer Res*. 2001;61(21):7747-7753.

26. Rozel S, Galban CJ, Nicolay K, et al. Synergy between anti-CCL2 and docetaxel as determined by DW-MRI in a metastatic bone cancer model. *J Cell Biochem*. 2009;107(1):58-64.

27. Lemasson B, Bouchet A, Maisin C, et al. Multiparametric MRI as an early biomarker of individual therapy effects during concomitant treatment of brain tumours. *NMR Biomed*. 2015;28(9):1163-1173.

28. Rieger J, Bahr O, Muller K, Franz K, Steinbach J, Hattingen E. Bevacizumab-induced diffusion-restricted lesions in malignant glioma patients. *J Neurooncol*. 2010;99(1):49-56.

29. Hakkarainen H, Sierra A, Mangia S, et al. MRI relaxation in the presence of fictitious fields correlates with myelin content in normal rat brain. *Magn Reson Med*. 2016;75(1):161-168.

SUPPORTING INFORMATION

Additional supporting information may be found online in the Supporting Information section at the end of this article.